Multiple scattering: The key to unravel the subwavelength world from the far-field pattern of a scattered wave

F. Simonetti*
Department of Mechanical Engineering, Imperial College, London SW7 2AZ, United Kingdom
(Received 4 December 2005; published 24 March 2006)

For more than a century the possibility of imaging the structure of a medium with diffracting wave fields has been limited by the tradeoff between resolution and imaging depth. While long wavelengths can penetrate deep into a medium, the resolution limit precludes the possibility of observing subwavelength structures. Near-field microscopy has recently demonstrated that the resolution limit can be overcome by bringing a probing sensor within one wavelength distance from the surface to be imaged. This paper extends the scope of near-field microscopy to the reconstruction of subwavelength structures from measurements performed in the far-field. It is shown that the distortion undergone by a wave field as it travels through an inhomogeneous medium and the subsequent generation of local evanescent fields encode subwavelength information in the far-field due to multiple scattering within the medium. This argument is proved theoretically and supported by a limited view experiment performed with elastic waves in which an image with a resolution better than a third of the wavelength is achieved.

DOI: 10.1103/PhysRevE.73.036619 PACS number(s): 42.30.−d, 43.60+d, 95.75.Mn

I. INTRODUCTION

Our visual perception of the outside universe is governed by the interaction between visible light and matter. Light scattered by objects or particles is detected by the eye-brain system to produce the perception of color (frequency) and contrast (intensity). On the other hand, light absorption, which limits the depth to which light can penetrate into matter, is the fundamental mechanism defining the extent to which the subsurface "world" can be sensed. As a result, while we can clearly appreciate the appearance of an opaque surface, we are not able to see through it. This leads to the *subsurface sensing problem* which is concerned with (i) the detection of objects embedded in opaque media, e.g., inclusions or flaws in a structure; (ii) the imaging of the shape of an object contained in a host medium, such as a foetus within the uterus; (iii) the formation of cross-sectional images of inhomogeneous media (tomography) as for brain imaging.

The first challenge in subsurface sensing is the definition of probing means able to penetrate media opaque to visible light. In this context, x-ray radiation has proved to be an invaluable tool since a broad range of materials such as biological tissues, dielectrics, and several metals are almost transparent to x-ray photons. Since the introduction of x rays in diagnostic medicine, much attention has been focused on the development of new methods including gamma rays, radionuclide, and nuclear magnetic resonance imaging (MRI). Another major contribution to subsurface sensing came after World War II when sonar and radar technologies became available. It was soon realized that the capability of these techniques to locate targets could be further exploited for imaging purposes. As a result, despite initial technical difficulties, ultrasound has been widely employed in medicine since the early seventies and today 25% of medical diagnostic imaging studies are performed with this technology [1].

Although the main drive for subsurface sensing can be attributed to medical diagnosis, several others fields such as geophysical surveying and nondestructive testing have benefited from and contributed to the development of this discipline. The approach to subsurface sensing in these areas can be different from that adopted in medical imaging due to constraints on materials and geometries. As an example, x-ray computerized tomography (CT) can provide very well defined images of the human body as it is possible to measure the transmission of x rays through the patient's body under different irradiation directions. However, there are circumstances in which the access to the surface of the volume to be imaged is limited. For instance, it is not possible to employ CT for imaging objects buried in the ground such as mines or archaeological artefacts, since transmission measurements are not feasible. For limited view subsurface sensing, microwave and ultrasound provide a substantial advantage compared to x ray due to the different nature of their interaction with matter. While x rays probe a medium by exploiting the particle nature of the electromagnetic radiation, microwave and ultrasound exhibit a stronger wave nature which is well described by Maxwell's equations and classical mechanics, respectively. As a consequence, ultrasonic and microwave reflection and diffraction phenomena, which in the case of x rays are significant at atomic scale only (Compton effect and Bragg scattering), project internal information all over the surface of the probed volume. Therefore a limited view of the scattered field can still lead to the retrieval of the internal structure of an object [2,3].

The principal notion in image formation is "resolution" which describes the ability of a system to resolve the smallest details in an object. Considerations on the wave nature of light led Ernst Abbe, more than one century ago, to introduce the diffraction limit later reformulated by Lord Rayleigh who showed that for a microscope the minimum resolvable size is in the order of the propagated wavelength λ (see, for in-

*Electronic address: f.simonetti@imperial.ac.uk

stance, Ref. [4]) regardless of the physical apparatus employed for the measurements, indeed a lens cannot focus over an area smaller than a square wavelength unless materials with negative refractive index are considered [5]. A limit of $\lambda/2$ was later established by Wolf in the case of full view tomographic reconstruction [6]. Implicit in the resolution limit is the fact that resolution can be increased by employing shorter wavelengths. However, as the wavelength decreases the penetration depth of the probing wave (either acoustic or electromagnetic) decreases due to increasing absorption and scattering. As a result, under the resolution limit constraint, the higher the resolution the shallower the volume of the object that can be imaged, this being the major limitation of current ultrasonic and electromagnetic wave imaging systems.

Over the past thirty years, the existence of the resolution limit has been challenged by progress made in microscopy, which has shown that by exploiting the super oscillatory properties of evanescent wave fields, resolution several orders of magnitude smaller than the wavelength can be achieved. The resolution limit, which is derived under the far-field (greater than λ) hypothesis, can be traced back to the fact that information associated with the subwavelength spatial periodicities of an object, which is encoded in the evanescent component of the field scattered by an object, is lost when the field is monitored far away from the object [7]. In other words, the propagation medium acts as a spatial filter of finite bandwidth which removes the spatial frequencies greater than $2\pi/\lambda$ (see, for instance, Goodman [4]). It was Synge who first suggested in 1928 that nonradiating fields produced by a subwavelength aperture could be used to enhance the resolution of optical microscopes [8]. The experimental evidence of Synge's idea came later in 1972 when Ash and Nicholls were able to achieve a "super resolution" of $\lambda/60$ in the microwave regime [9]. During the early eighties the use of nonradiating fields revolutionized microscopy leading to the introduction of the first near-field scanning optical microscope by Lewis *et al.* [10] and Dürig *et al.* [11]. Since then enormous progress has been made and near-field scanning optical microscopy (NSOM) has become an established discipline (see, for instance, Betzig *et al.* [12], Lewis *et al.* [13], and a recent book by Courjon [14]).

The fundamental practical challenge in NSOM is represented by the need for at least one of the probing sensors to be within one wavelength distance from the sample surface; indeed the closer the sensor the higher the resolution [15]. For instance, under the illumination mode configuration the sample is probed with an evanescent wave excited in the near-field of the sample and the radiating component of the scattered field is detected remotely in the far-field. Conversely, in the collection mode, radiating fields are excited from the far-field and scattered evanescent waves are measured in the near field. In either case the key phenomenon is the conversion of evanescent waves into radiating ones and vice versa, by tunneling [16].

The progress made in near-field microscopy naturally raises the question whether super resolution can also be achieved when all the probing sensors are placed in the far-field. This is crucial to breaking the wavelength constraint which dictates the tradeoff between resolution and imaging depth with current subsurface sensing technology. In 1998 Chen and Chew [17] have reported on a set of microwave experiments in which dielectric targets were imaged from the far-field by means of a radar system. They showed that by taking into account multiple scattering in the imaging algorithm super resolved images could be obtained. A qualitative explanation was provided based on the argument that the evanescent waves generated within an inhomogeneous medium as a radiating wave travels through it are converted into radiating waves by multiple scattering. Since evanescent waves contain super resolution information, multiple scattering encodes super resolution in the far-field. This idea was further explored by Cui *et al.* [18] within the framework of nonlinear inversion algorithms. In a recent paper, Belebir *et al.* [19] have demonstrated numerically that the resolution of near-field techniques, such as total internal reflection tomography [20], is also enhanced by multiple scattering. In the context of time reversal focusing, it has been shown that while the resolution of the time reversal mirror [21] in a homogeneous medium is limited by the classical Rayleigh limit, the method achieves super resolution in random media due to multiple scattering (see, for instance, Ref. [22]). Although there is experimental and numerical evidence of the role of multiple scattering in super resolution imaging, it is not yet clear how the subwavelength structure of the probed medium is linked to far-field measurements and how multiple scattering encodes super resolution in the outgoing radiating waves.

The aim of this paper is twofold: first to provide a general theoretical framework for far-field super resolution in the light of recent numerical and experimental results, second to produce further experimental evidence for the limited view case. The framework, which is based on the well known T-matrix formalism [23], enables the characterization of the encoding of subwavelength information in the far-field pattern of a scattered wave by multiple scattering and leads to a clear link between far-field measurements and the subwavelength structure of the probed medium. Moreover, it is proposed and shown experimentally that a class of reconstruction methods introduced by Colton and Kirsch (see for a recent review of the subject Ref. [24]) can lead to super resolution imaging.

After formulating the imaging problem in Sec. II the T-matrix formalism and its implications for image formation are discussed in Sec. III. To the first order approximation the formalism leads to the Born approximation, which is the model currently used in imaging theory to represent the interaction between probing waves and objects. By observing that this approximation results in the resolution limit, Sec.IV reviews the main approaches to super resolution with a particular emphasis on total internal reflection tomography, and points out that the range of validity of the Born approximation can be very limited. Section V builds on the results of Sec. III, and shows how abandoning the Born approximation and considering multiple scattering can lead to the retrieval of super resolution information from far-field measurements. However, the price to pay is the need for solving a nonlinear inverse problem. A direct application of the argument proposed in Sec. V is provided in Sec. VI for the shape reconstruction problem, for which the nonlinear inverse problem

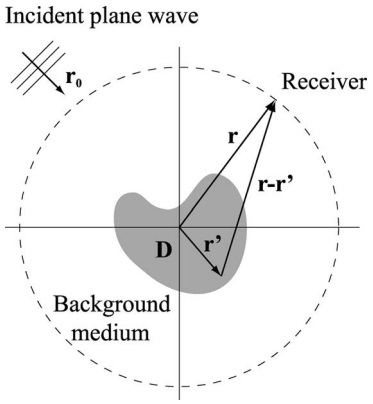

FIG. 1. Schematic of the model for tomographic reconstruction. The object is probed from the far-field by means of an incident plane wave. The scattered field is measured with a receiver in the far-field.

can be replaced with a simpler linear one. Finally, Sec. VII reports on a limited view experiment performed with elastic waves which demonstrates a resolution better than $\lambda/3$ without the need for *a priori* information about the scatterer shape.

II. IMAGING AND RESOLUTION

The general imaging problem can be formulated in terms of reconstructing the spatial distribution of one or more physical parameters which characterize the structure of the object being probed. The measurement scenario can comprise a background medium where the probing sensors are placed and the object which can be either finite or infinite. As an example, Fig. 1 shows the classical configuration for tomographic reconstruction, in which the object is finite and is immersed in a homogeneous background. The object is illuminated from different directions and for each of them the scattered field is measured at various angles. In this paper it is assumed that the scattering problem is described by a scalar wave field, ψ, solution to

$$\hat{H}\psi(\mathbf{r},k\hat{\mathbf{r}}_0,\omega) = -k^2 O(\mathbf{r},\omega)\psi(\mathbf{r},k\hat{\mathbf{r}}_0,\omega); \tag{1}$$

where $\hat{H}$ is the Helmholtz operator (∇^2+k^2), k is the background wave number $(2\pi/\lambda)$, $\hat{\mathbf{r}}_0$ specifies the direction of the incident plane wave which illuminates the object and ω is the angular frequency. The object is described by the so called *object function*, $O(\mathbf{r},\omega)$, of support D corresponding to the volume occupied by the object. $O(\mathbf{r},\omega)$ depends on the type of wave field used to probe the object: for electromagnetic wave sensing it is related to the index of refraction [25], $n(\mathbf{r},\omega)$, through the relation $O(\mathbf{r})=n^2(\mathbf{r},\omega)-1$, for thermal waves it depends on the thermal diffusivity [26], for acoustic waves it is linked to density and compressibility [27]. It can also be observed that Eq. (1) is analogous to the time independent Schrödinger equation for the scattering of nonrelativistic particles by a conservative potential $O(\mathbf{r})$ (see, for instance, Ref. [28]). The dependence of the object function on ω is due to dispersion and energy dissipation phenomena. The analysis performed in the rest of this paper will consider monochromatic wave fields, therefore the explicit dependence on ω is omitted.

The imaging problem consists of reconstructing the function $O(\mathbf{r})$ from a set of experiments, the quality of the reconstruction being dependent on its resolution. In this paper, the criterion adopted to evaluate the resolution is based on the representation of the object function in the spatial frequency domain $\mathbf{\Omega}$, which is obtained by performing the three-dimensional Fourier transform of $O(\mathbf{r})$,

$$\tilde{O}(\mathbf{\Omega}) = \int_{-\infty}^{\infty} d^3 r O(\mathbf{r}) e^{-i\mathbf{\Omega}\cdot\mathbf{r}}. \tag{2}$$

Any imaging system provides an interpretation of the object function, $\tilde{R}(\mathbf{\Omega})$, which, in general, differs from the actual $\tilde{O}(\mathbf{\Omega})$ due to the presence of noise and the limited resolving power of the imaging system. While noise can affect the entire spectrum of $\tilde{O}(\mathbf{\Omega})$, the lack of resolution results in the loss of higher spatial frequencies. In this context, the classical resolution limit states that it is not possible to reconstruct spatial periodicities shorter than $\lambda/2$ [6] (i.e., $|\mathbf{\Omega}|>4\pi/\lambda$). Any image which contains spatial periodicities shorter than $\lambda/2$ is said to be super resolved.

III. SCATTERING FORMALISM

This section summarizes the main results of the T-matrix formalism [23] used in the theory of quantum scattering and reinterprets them in the light of the subsurface sensing problem. Let us consider the integral representation of Eq. (1) which is known as the Lippman-Schwinger equation,

$$\psi(\mathbf{r},k\hat{\mathbf{r}}_0) = \exp(ik\hat{\mathbf{r}}_0\cdot\mathbf{r}) - k^2\int_D d^3 r' G(\mathbf{r},\mathbf{r}')O(\mathbf{r}')\psi(\mathbf{r}',k\hat{\mathbf{r}}_0), \tag{3}$$

where the first term of the right hand side is the incident plane wave which illuminates the object and $G(\mathbf{r},\mathbf{r}')$ is the free-space Green's function,

$$G(\mathbf{r},\mathbf{r}') = -\frac{\exp(ik|\mathbf{r}-\mathbf{r}'|)}{4\pi|\mathbf{r}-\mathbf{r}'|}, \tag{4}$$

which is a solution to $\hat{H}G(\mathbf{r},\mathbf{r}')=\delta(|\mathbf{r}-\mathbf{r}'|)$. In the far-field $G(\mathbf{r},\mathbf{r}')$ can be approximated by means of the paraxial approximation, $|\mathbf{r}-\mathbf{r}'|\to r[1-(\mathbf{r}\cdot\mathbf{r}')/r^2]$, hence

$$\lim_{r\to\infty} G(\mathbf{r},\mathbf{r}') = -\frac{e^{ikr}}{4\pi r}e^{-ik\hat{\mathbf{r}}\cdot\mathbf{r}'}. \tag{5}$$

By substituting Eq. (5) into Eq. (3) the total field can be expressed as

$$\lim_{r\to\infty}\psi(\mathbf{r},k\hat{\mathbf{r}}_0) = e^{ik\hat{\mathbf{r}}_0\cdot\mathbf{r}} + k^2 f(k\hat{\mathbf{r}},k\hat{\mathbf{r}}_0)\frac{e^{ikr}}{4\pi r}, \tag{6}$$

where $f(k\hat{\mathbf{r}},k\hat{\mathbf{r}}_0)$ is the scattering amplitude defined as

$$f(k\hat{\mathbf{r}},k\hat{\mathbf{r}}_0)=\int_D d^3r' e^{-ik\hat{\mathbf{r}}\cdot\mathbf{r}'}O(\mathbf{r}')\psi(\mathbf{r}',k\hat{\mathbf{r}}_0). \tag{7}$$

Through Eq. (6), the scattering amplitude can be measured experimentally, by illuminating the object from all possible directions $\hat{\mathbf{r}}_0$ and for each of them detecting the scattered field in all directions $\hat{\mathbf{r}}$, both illumination and detection being performed in the far-field. Let us define the V matrix, $V(\alpha\hat{\mathbf{u}},k\hat{\mathbf{r}}_0)$, as

$$V(\gamma\hat{\mathbf{c}},\beta\hat{\mathbf{b}})=\int_D d^3r' e^{-i\gamma\hat{\mathbf{c}}\cdot\mathbf{r}'}O(\mathbf{r}')e^{i\beta\hat{\mathbf{b}}\cdot\mathbf{r}'}. \tag{8}$$

If $\gamma\hat{\mathbf{c}}$ and $\beta\hat{\mathbf{b}}$ are both real, the V matrix is equivalent to the three-dimensional Fourier transform, $\tilde{O}(\Omega\mathbf{e})$, of the object function calculated at the spatial frequency $\Omega\mathbf{e}=\gamma\hat{\mathbf{c}}-\beta\hat{\mathbf{b}}$, in particular

$$V(k\hat{\mathbf{r}},k\hat{\mathbf{r}}_0)=\tilde{O}(k(\hat{\mathbf{r}}-\hat{\mathbf{r}}_0)). \tag{9}$$

In the $\mathbf{\Omega}$ space, it can be observed that for a prescribed illumination direction $\hat{\mathbf{r}}_0$ the scattering amplitude $f(k\hat{\mathbf{r}},k\hat{\mathbf{r}}_0)$ is defined over a shell whose radius is k. This shell is known as the Ewald shell [29].

In order to proceed to the development of the formalism, the T matrix or transition amplitude [23] is introduced,

$$T(\alpha\hat{\mathbf{u}},k\hat{\mathbf{r}}_0)=\int_D d^3r' e^{-i\alpha\hat{\mathbf{u}}\cdot\mathbf{r}'}O(\mathbf{r}')\psi(\mathbf{r}',k\hat{\mathbf{r}}_0), \tag{10}$$

so that $T(\alpha\hat{\mathbf{u}},k\hat{\mathbf{r}}_0)=f(k\hat{\mathbf{r}},k\hat{\mathbf{r}}_0)$ for $\alpha\hat{\mathbf{u}}=k\hat{\mathbf{r}}$. The T matrix is said to be on the shell if $\alpha\hat{\mathbf{u}}=k\hat{\mathbf{r}}$, off the shell otherwise. The exact Green's function (4) can be expressed by means of its eigenfunction expansion,

$$G(\mathbf{r},\mathbf{r}')=-\frac{1}{8\pi^3}\int_{-\infty}^{+\infty}d^3\alpha\frac{\exp\{[i\alpha\hat{\mathbf{u}}\cdot(\mathbf{r}-\mathbf{r}')]\}}{k^2-\alpha^2+i\epsilon}, \tag{11}$$

which substituted into Eq. (3) after some manipulations leads to an integral equation for the T matrix [28],

$$T(k\hat{\mathbf{r}},k\hat{\mathbf{r}}_0)=V(k\hat{\mathbf{r}},k\hat{\mathbf{r}}_0)+\frac{k^2}{8\pi^3}\int_{-\infty}^{+\infty}d^3\alpha\frac{V(\hat{\mathbf{r}},\alpha\hat{\mathbf{u}})T(\alpha\hat{\mathbf{u}},k\hat{\mathbf{r}}_0)}{k^2-\alpha^2+i\epsilon}. \tag{12}$$

Note that this expression is valid both in the near and far-field, since the exact expression for the Green's function (11) is used to obtain Eq. (12). The quantity $i\epsilon$ in Eqs. (11) and (12) is an infinitesimal value introduced to remove the singularity when $k^2=\alpha^2$ (see, for instance, Ref. [30]).

Equation (12) implies that for a prescribed illumination direction $\hat{\mathbf{r}}_0$, the T matrix on the shell, $T(k\hat{\mathbf{r}},k\hat{\mathbf{r}}_0)$, is given by the V matrix on the shell, $V(k\hat{\mathbf{r}},k\hat{\mathbf{r}}_0)$, plus an integral term which also depends on the off the shell elements of the V matrix and the T matrix. Each of these quantities has a precise physical meaning; the T matrix on the shell corresponds to the far-field measurements [compare Eqs. (10), (7), and (6)], whereas the V matrix on the shell corresponds to the Fourier transform of the object function given by Eq. (9). Equation (9) implies that for all the possible combinations of illumination and detection directions, $\hat{\mathbf{r}}_0$ and $\hat{\mathbf{r}}$, the V matrix defines the object Fourier transform within a sphere of radius $2k$ which is the limiting Ewald's sphere. On the other hand, the off the shell elements of the V matrix correspond to spatial frequencies of the object which can assume any value in the $\mathbf{\Omega}$ space. The off the shell elements of the T matrix, which are not measurable in the far-field, account for the interaction between the field ψ and $O(\mathbf{r})$ inside the object.

IV. BORN APPROXIMATION

To the first order approximation the solution to Eq. (12) can be obtained by neglecting the integral term

$$T^{(1)}(k\hat{\mathbf{r}},k\hat{\mathbf{r}}_0)\approx V(k\hat{\mathbf{r}},k\hat{\mathbf{r}}_0), \tag{13}$$

which is equivalent to replacing the field ψ in Eq. (10) with the incident wave, $\exp(ik\hat{\mathbf{r}}_0\cdot\mathbf{r})$, it therefore represents the classical Born approximation for weakly scattering media. This approximation provides a direct solution to the inverse problem, because the V matrix, and therefore $\tilde{O}(\mathbf{\Omega})$ inside the limiting Ewald's sphere, can be obtained from the on the shell T matrix, which corresponds to the far-field measurements. This means that under ideal conditions of measurements performed for all the possible $\hat{\mathbf{r}}_0$ and $\hat{\mathbf{r}}$ combinations (full view configuration) and in the absence of noise, the reconstructed object function is given by

$$\tilde{R}(\mathbf{\Omega})=H(\mathbf{\Omega})\tilde{O}(\mathbf{\Omega}), \tag{14}$$

where $H(\mathbf{\Omega})$ is a low-pass filter defined as

$$H(\mathbf{\Omega})=\begin{cases}1, & |\mathbf{\Omega}|<2k\\ 0, & |\mathbf{\Omega}|>2k.\end{cases} \tag{15}$$

This implies that it is not possible to recover spatial frequencies greater than $2k$, hence the classical resolution limit $\lambda/2$ is established [6]. Equation (14) implies that the reconstructed object function in the geometric space, $R(\mathbf{r})$, can be expressed as the convolution of the real object function and the point spread function $h(\mathbf{r})$,

$$R(\mathbf{r})=\int_D d^3\mathbf{r}' h(\mathbf{r}-\mathbf{r}')O(\mathbf{r}'), \tag{16}$$

where

$$h(\mathbf{r})=\frac{4k^3}{\pi^2}\left[\frac{J_1(2k|\mathbf{r}|)}{2k|\mathbf{r}|}\right]. \tag{17}$$

$h(\mathbf{r})$ is the inverse Fourier transform of the filter $H(\mathbf{\Omega})$, $J_1(\cdot)$ being the spherical Bessel function of the first order.

A. Super resolution

Under the Born approximation there are two approaches to super resolution. The first is based on the analyticity of the function $\tilde{O}(\mathbf{\Omega})$ when the support D is finite. In this case, $\tilde{O}(\mathbf{\Omega})$ can be extrapolated to the exterior of the limiting Ewald's sphere by analytic continuation [30] so achieving

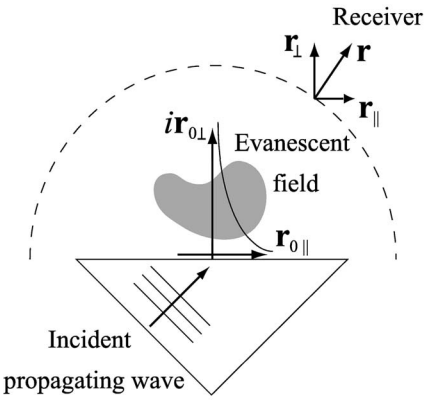

FIG. 2. Schematic of the TIRT configuration. The object is probed with an evanescent field generated by total internal reflection by means of a prism. The radiating field scattered by the object is detected remotely.

unlimited resolution. This is equivalent to deconvolving $O(\mathbf{r})$ from Eq. (16) given the knowledge of the point spread function $h(\mathbf{r})$. However, as observed by several authors [31–35], analytic continuation is not practically feasible due to its severe instability and high sensitivity to noise.

A second approach to super resolution consists of applying the near-field scanning optical microscopy (NSOM) principles to tomographic reconstruction. As a result, in order to exploit the super oscillatory properties of evanescent waves the object needs to be placed within one wavelength distance from the probing system. It should be emphasized that a common problem with NSOM imaging is that it provides a two-dimensional map of the three-dimensional internal structure of the object. This can lead to considerable difficulties in interpreting and analyzing the significance of a NSOM image [36,37]. On the other hand, near-field tomography can retrieve the three-dimensional structure of the object maintaining the super resolving capabilities of NSOM [38–40]. One of the techniques which has attracted considerable interest is total internal reflection tomography [20,41,42] (TIRT). In this case, the object is illuminated with an evanescent wave obtained by total internal reflection within a prism of suitable index of refraction as shown in Fig. 2. The radiating component of the field scattered by the object is detected remotely in the far-field. Since the illuminating wave is evanescent $\hat{\mathbf{r}}_0$ is complex,

$$\hat{\mathbf{r}}_0 = \hat{\mathbf{r}}_{0\parallel} + i\hat{\mathbf{r}}_{0\perp} \quad \text{with } \hat{\mathbf{r}}_0 \cdot \hat{\mathbf{r}}_0 = 1, \tag{18}$$

where $(\cdot)$ is the inner product in $\mathbb{C}^3$. As a result, $V(k\hat{\mathbf{r}}, k\hat{\mathbf{r}}_0)$ in Eq. (13) can be thought of as the analytic continuation of the object function Fourier transform in the complex space, thus

$$T^{(1)}(k\hat{\mathbf{r}}, k\hat{\mathbf{r}}_0) = \widetilde{O}[k(\hat{\mathbf{r}}_\parallel - \hat{\mathbf{r}}_{0\parallel}) + k(\hat{\mathbf{r}}_\perp - i\hat{\mathbf{r}}_{0\perp})]. \tag{19}$$

Note that implicit in Eq. (19) is the conversion of the evanescent field into radiating waves caused by the linear interaction between the evanescent wave and the object. The super resolving capabilities of TIRT are explained by observing that the analytic continuation of $\widetilde{O}(\mathbf{\Omega})$ in the complex space is equivalent to [39]

$$\widetilde{O}[k(\hat{\mathbf{r}}_\parallel - \hat{\mathbf{r}}_{0\parallel}) + k(\hat{\mathbf{r}}_\perp - i\hat{\mathbf{r}}_{0\perp})] = \int_{-\infty}^{+\infty} d\Omega_\perp \widetilde{O}[k(\hat{\mathbf{r}}_\parallel - \hat{\mathbf{r}}_{0\parallel}) + \Omega_\perp] I(\Omega_\perp, \hat{\mathbf{r}}_\parallel, \hat{\mathbf{r}}_{0\parallel}) \tag{20}$$

therefore

$$T^{(1)}(k\hat{\mathbf{r}}, k\hat{\mathbf{r}}_0) = \int_{-\infty}^{+\infty} d\Omega_\perp \widetilde{O}[k(\hat{\mathbf{r}}_\parallel - \hat{\mathbf{r}}_{0\parallel}) + \Omega_\perp] I(\Omega_\perp, \hat{\mathbf{r}}_\parallel, \hat{\mathbf{r}}_{0\parallel}), \tag{21}$$

where $\mathbf{\Omega}_\perp \in \mathbb{R}^3$ and $I(\cdot)$ is a kernel defined by Fischer [39]. For given illumination and detection directions ($\hat{\mathbf{r}}$ and $\hat{\mathbf{r}}_0$), the far-field measurement contains information about the infinite spatial frequencies $\mathbf{\Omega}$ satisfying the conditions

$$\hat{\mathbf{r}}_{0\parallel} \cdot \mathbf{\Omega} = 0 \quad \text{and} \quad \hat{\mathbf{r}}_\parallel \cdot \mathbf{\Omega} = 0. \tag{22}$$

This is the very mechanism which enables the encoding of super resolution information in far-field measurements. However, while in the case of propagating wave illumination, there is a one-to-one correspondence between the measurements and $\widetilde{O}(\mathbf{\Omega})$ [see Eq. (13)] in TIRT a single measurement corresponds to infinite possible values of $\widetilde{O}(\mathbf{\Omega})$. Although the inverse problem of retrieving $\widetilde{O}(\mathbf{\Omega})$ from a set of measurements is ill-posed in the sense of Hadamard [43], the solution can be obtained via the singular value decomposition of a linearized scattering kernel as shown by Carney and Schotland [42].

B. Born approximation validity

The validity of the Born approximation is crucial to the accuracy of Eqs. (13) and (16) and it has been the subject of extensive research in conjunction with the Rytov approximation [44] (which is not discussed in this paper for brevity). The hypothesis of a weakly scattering medium ensures that multiple scattering is negligible, hence the field within the object can be replaced by the incident wave. However, the question arises as to how to define a weakly scattering medium. An early computational study by Azimi and Kak [45] suggested that even when the contrast between the inhomogeneities and the background (which is equivalent to the object function) is as small as 5% multiple scattering can lead to significant distortions in the reconstruction. It is now well established that the distortion is not only due to contrast [46], but it also depends on the size of the object relative to the wavelength [47–49]. In particular, it is found that for the Born approximation to be valid the object function has to satisfy the condition

$$\sup_{r<\rho} |O(\mathbf{r})| < c\frac{\lambda}{\rho}, \tag{23}$$

where ρ is the characteristic size of the object and c is a constant for which different values have been proposed [47,49]. In a recent paper, Natterer [50] has derived an error bound for the Born approximation which bases the constant c

on an exact mathematical theory. The main implication of Eq. (23) is that even when the contrast is low, multiple scattering cannot be neglected if the object is large compared to the wavelength.

V. MULTIPLE SCATTERING

As discussed in the previous section, under the Born approximation, it is not possible to retrieve spatial frequencies higher than $2k$ from far-field measurements [Eqs. (14) and (15)]. In turn, Eq. (13) implies that these frequencies are *invisible* from the far-field since they do not scatter the incident wave, this being the very physical reason for the existence of the resolution limit. However, it can be observed that this conclusion is a consequence of the Born approximation only. If multiple scattering is taken into account, the scattered field is given by

$$T(k\hat{\mathbf{r}},k\hat{\mathbf{r}}_0) = \widetilde{O}[k(\hat{\mathbf{r}}-\hat{\mathbf{r}}_0)] + \frac{k^2}{8\pi^3} \times \int_{-\infty}^{+\infty} d^3\alpha \frac{\widetilde{O}(k\hat{\mathbf{r}}-\alpha\hat{\mathbf{u}})T(\alpha\hat{\mathbf{u}},k\hat{\mathbf{r}}_0)}{k^2-\alpha^2+i\epsilon}. \quad (24)$$

which is Eq. (12) written in terms of $\widetilde{O}(\mathbf{\Omega})$. Multiple scattering results in the presence of the additional integral term on the right hand side. Since the integral is carried out in $\mathbb{R}^3$, a single measurement (fixed $k\hat{\mathbf{r}}$ and $k\hat{\mathbf{r}}_0$) depends on all the spatial frequencies of $\widetilde{O}(\mathbf{\Omega})$. As a consequence, multiple scattering encodes super resolution information in the far-field by means of the integral term in Eq. (24) in a similar fashion to the encoding produced by evanescent waves in TIRT. This concept can be further clarified by considering the second order scattering. In this case the field within the object can be approximated as

$$\psi(\mathbf{r}',k\hat{\mathbf{r}}_0) \approx \exp(ik\hat{\mathbf{r}}_0\cdot\mathbf{r}') - k^2\int_D d^3r'' G(\mathbf{r}',\mathbf{r}'') \times O(\mathbf{r}'')\exp(ik\hat{\mathbf{r}}_0\cdot\mathbf{r}''), \quad (25)$$

which substituted into Eq. (10) gives

$$T(k\hat{\mathbf{r}},k\mathbf{r}_0) = \widetilde{O}[k(\hat{\mathbf{r}}-\hat{\mathbf{r}}_0)] - k^2\int_D d^3r'' \int_D d^3r' e^{-ik\hat{\mathbf{r}}\cdot\mathbf{r}'} O(\mathbf{r}')G(\mathbf{r}',\mathbf{r}'') \times [O(\mathbf{r}'')e^{ik\hat{\mathbf{r}}_0\cdot\mathbf{r}''}]. \quad (26)$$

Let us consider the integral over $\mathbf{r}'$. For a given $\mathbf{r}''$, this integral is equivalent to the first order scattering due to the incident field $G(\mathbf{r}',\mathbf{r}'')[O(\mathbf{r}'')e^{ik\hat{\mathbf{r}}_0\cdot\mathbf{r}''}]$, which corresponds to the field excited by a *virtual* point source at $\mathbf{r}''$. Since the field of a point source can be expanded in a superposition of infinite radiating and evanescent plane waves (for instance by using the Weyl expansion [51]), the virtual source behaves as the subwavelength aperture used in the illumination mode of a near-field microscope. As in NSOM, the evanescent waves associated with $G(\mathbf{r}',\mathbf{r}'')$, are converted into radiating waves by the points of the object in the near field of $\mathbf{r}''$, i.e., $|\mathbf{r}'-\mathbf{r}''|<\lambda$. The encoding of the subwavelength information carried by the evanescent components of $G(\mathbf{r},\mathbf{r}'')$ can be expressed analytically by substituting the eigenfunction expansion for the Green's function (11) into (26),

$$T^{(2)}(k\hat{\mathbf{r}},k\hat{\mathbf{r}}_0) = \widetilde{O}[k(\hat{\mathbf{r}}-\hat{\mathbf{r}}_0)] + \frac{k^2}{8\pi^3}\int_{-\infty}^{+\infty} d^3\alpha \times \frac{\widetilde{O}[k\hat{\mathbf{r}}-\alpha\hat{\mathbf{u}}]\widetilde{O}[\alpha\hat{\mathbf{u}}-k\hat{\mathbf{r}}_0]}{k^2-\alpha^2+i\epsilon}, \quad (27)$$

which clearly shows the dependence of $T(k\hat{\mathbf{r}},k\hat{\mathbf{r}}_0)$ on all the spatial frequencies of $\widetilde{O}(\mathbf{\Omega})$.

The first important result of this paper can be expressed as follows: while under the Born approximation far-field measurements are sensitive to the spatial frequencies contained within the Ewald limiting sphere only, multiple scattering and the subsequent conversion of evanescent fields into propagating waves is the fundamental mechanism which makes spatial frequencies larger than 2k *visible* from the far-field. Indeed, for subwavelength features to be visible, the inverse problem expressed by Eq. (24) or equivalently by Eq. (1) needs to be solved with respect to the object function, the problem being nonlinear and ill-posed in the sense of Hadamard [43].

Since the introduction of regularization methods for ill-posed problems by Tikhonov in 1963 [52], the problem has attracted considerable interest across the mathematical community which has addressed the conditions of existence and uniqueness of the solution. For a comprehensive overview of the topic the reader is referred to the monograph by Colton and Kress [53]. According to Luke and Potthast [54] there are three fundamental approaches to solve the ill-posed, nonlinear inverse problem. The first consists of tackling it directly by means of iterative methods of gradient or Newton type (a list of references is provided by Potthast [55]). Among these the distorted Born iterative method [56] has led to the super resolution results reported by Chen and Chew [17]. The second category splits the inverse problem into a linear ill-posed problem of determining the scattered field in the exterior of the object from the measured far-field, and the well-posed problem of finding the boundary of the object, ∂D, or the object function from the scattered field (references can be found in Ref. [54]). The third method goes under the name of linear sampling method (LSM) and was introduced by Colton and Kirsch in 1996 [57,58]. The method is limited to the reconstruction of the support D of the object function, i.e., the shape of the object. The nonlinear inverse problem is replaced with a linear integral equation of the first kind and no assumptions on the object nature are made. The method is considered in greater detail in the next section since it provides further insight into the super resolution argument discussed in this section.

As a last remark it is emphasized that multiple scattering represents a source of coherent noise for reconstruction methods based on the Born approximation due to the additional integral term to Eq. (13) [compare with Eq. (24)]. Here, the term coherent is used to stress the deterministic

nature of multiple scattering. Kolobov and Fabre [59] have discussed the ultimate resolution limit in optical imaging in the framework of analytic continuation and have shown that unlimited resolution is not possible due to the noise induced by the quantum fluctuations of light. In this paper, it is argued that unlimited resolution by analytic continuation is inherently impossible in a classical sense, because of multiple scattering.

VI. SHAPE RECONSTRUCTION

This section considers the problem of reconstructing the shape of one or more objects from far-field data. In this context, resolution refers to how detailed the reconstruction of the object boundary is. As mentioned in the previous section, Colton and Kirsch [57,58] have introduced a simple method which replaces the ill-posed nonlinear inverse problem with a linear integral equation. The method is based on the far-field T-matrix operator $T_\infty: L^2(\mathbb{S}) \to L^2(\mathbb{S})$,

$$T_\infty|y\rangle = \int_{\mathbb{S}} ds(\hat{\mathbf{r}}_0) f(k\hat{\mathbf{r}}, k\hat{\mathbf{r}}_0) y(k\hat{\mathbf{r}}_0), \tag{28}$$

where $\mathbb{S}$ is the unit shell in $\mathbb{R}^3$ and the ket symbol is used according to the Dirac bra-ket notation [30]. As discussed in Sec. III the operator can be built by measuring the scattered field experimentally. The idea of the LSM is to consider the solution to the equation

$$T_\infty|y_{\mathbf{z}}\rangle = |g_{\mathbf{z}}\rangle, \tag{29}$$

where the function $g_{\mathbf{z}} \in L^2(\mathbb{S})$ is defined as

$$g_{\mathbf{z}}(k\hat{\mathbf{r}}) = e^{-ik\hat{\mathbf{r}}\cdot\mathbf{z}}. \tag{30}$$

It can be shown that the $L^2(\mathbb{S})$ norm of the solution, $\sqrt{\langle y_{\mathbf{z}}|y_{\mathbf{z}}\rangle}$, becomes unbounded as $\mathbf{z}$ approaches the boundary of the object, ∂D. Therefore ∂D can be found by evaluating the function $\sqrt{\langle y_{\mathbf{z}}|y_{\mathbf{z}}\rangle}$ in a grid of $\mathbb{R}^3$ containing the object, ∂D being given by the locus of points $\mathbf{z}$ where $\sqrt{\langle y_{\mathbf{z}}|y_{\mathbf{z}}\rangle}$ increases sharply. A modified version of the LSM, known as the factorization method (FM), was proposed by Kirsch in 1998 [60] who considered the equation

$$(T_\infty^\dagger T_\infty)^{1/4}|y_{\mathbf{z}}\rangle = |g_{\mathbf{z}}\rangle, \tag{31}$$

where $T_\infty^\dagger$ is the adjoint of T_∞ in $L^2(\mathbb{S})$; note that the operator $T_\infty^\dagger T_\infty$ corresponds to the time reversal operator introduced by Prada *et al.* [61]. For lossless media [i.e., real $O(\mathbf{r})$] Kirsch showed that a point $\mathbf{z}$ belongs to D if and only if Eq. (31) is solvable. This condition can be assessed by considering the singular value decomposition of T_∞. The operator is compact [53] and therefore has a countable number of discrete eigenvalues accumulating only at zero. Moreover, since $O(\mathbf{r})$ is real T_∞ is normal. As a result, there exists an orthonormal basis $\{v^n\}$ for $L^2(\mathbb{S})$ consisting of eigenfunctions of T_∞ as shown by Mast *et al.* [62]

$$T_\infty|v^n\rangle = \mu_n|v^n\rangle, \tag{32}$$

or equivalently

$$T_\infty^\dagger T_\infty|v^n\rangle = |\mu_n|^2|v^n\rangle, \tag{33}$$

which means that $\{|\mu_n|, |v^n\rangle, \mathrm{sgn}(\mu_n)|v^n\rangle\}$ is a singular system for T_∞. By virtue of Picard's theorem [53] Eq. (31) is solvable if and only if

$$\sum_{n=1}^{\infty} \frac{1}{|\mu_n|} |\langle g_{\mathbf{z}}|v_{\mathbf{z}}^n\rangle|^2 < \infty. \tag{34}$$

In a similar fashion to the reconstruction procedure of the LSM, the support of the object function D is the locus of points $\mathbf{z}$ for which Eq. (34) is finite, i.e.,

$$\mathbf{z} \in D \Leftrightarrow P(\mathbf{z}) = \left(\sum_{n=1}^{\infty} \frac{1}{|\mu_n|} |\langle g_{\mathbf{z}}|v_{\mathbf{z}}^n\rangle|^2 \right)^{-1} > 0, \tag{35}$$

where $P(\mathbf{z})$ is referred to as the pseudo spectrum.

Clearly in the absence of noise, Eq. (35) leads to a reconstruction of the object shape with unlimited resolution. This is a consequence of the general conditions under which Eq. (35) is derived, i.e., the nonlinear scattering problem described by Eq. (1) for lossless media. Neither the Born approximation nor particular boundary conditions on ∂D are assumed. This confirms the argument discussed in the previous section and demonstrates how abandoning the Born approximation and including multiple scattering leads to super resolution.

A. Pointlike scatterers

In order to gain further insight into how the nonlinearity of the inverse problem, which is only due to multiple scattering, is embedded in the linear method provided by Eq. (31), the case of an object made of a collection of M isotropic pointlike scatterers is considered. The object function can be expressed as

$$O(\mathbf{r}) = \sum_{m=1}^{M} o_m \delta(\mathbf{r} - \mathbf{r}_m), \tag{36}$$

where o_m and $\mathbf{r}_m$ represent the scattering coefficient and position of the mth scatterer, respectively. It can be shown that T_∞ only has M nonzero eigenvalues [63]. The infinite eigenfunctions $|\varphi^n\rangle$ associated with the zero eigenvalue satisfy the eigenequation

$$T_\infty|\varphi^n\rangle = 0. \tag{37}$$

Since the zero eigenvalue has infinite multiplicity, Eq. (34) is always singular unless $\langle g_{\mathbf{z}}|\varphi^n\rangle$ vanishes. As a consequence, condition (35) is equivalent to

$$\mathbf{z} \in D \Leftrightarrow \langle g_{\mathbf{z}}|\varphi_{\mathbf{z}}^n\rangle = 0, \quad \forall \ n > M. \tag{38}$$

It is interesting to give a direct proof of the forward condition. By comparing Eq. (28) with Eq. (6) it can be observed that $T_\infty|y\rangle$ is the far-field pattern of the scattered field due to a linear combination of incident plane waves, $\exp(ik\hat{\mathbf{r}}_0\cdot\mathbf{z})$,

with relative amplitude $y(k\hat{\mathbf{r}}_0)$, the total incident field being $\langle g_{\mathbf{z}}|y\rangle$. Therefore Eq. (37) implies that if the object is probed with the incident field $\langle g_{\mathbf{z}}|\varphi^n\rangle$ the scattered field vanishes. This can only happen if the field $\langle g_{\mathbf{z}}|\varphi^n\rangle$ vanishes at the points $\mathbf{z}=\mathbf{r}_m$ for any to $m \in \{1,\ldots,M\}$. Indeed, the field scattered by a point scatterer is proportional to the total field at that point [64]. So if the incident field vanishes at all the scatterer centers simultaneously, it is not perturbed by them and no energy is scattered. As a result, if $\mathbf{z}$ coincides with one of the scattering centers $\mathbf{r}_m$,$\langle g_{\mathbf{z}}|\varphi^n\rangle$ vanishes for any $|\varphi^n\rangle$, this being true whether or not multiple scattering is considered in the forward problem. Therefore it is proved that for pointlike scatterers, the forward condition of Eq. (38) [hence Eq. (35)] holds in the presence of multiple scattering. Moreover, the problem becomes linear because the reconstruction is based on those wave fields which are not scattered.

It can be observed that Eq. (38) implies that the following condition:

$$\mathbf{z} \in D \Leftrightarrow E(\mathbf{z}) = \left(\sum_{n=M+1}^{\infty} |\langle g_{\mathbf{z}}|\varphi_{\mathbf{z}}^n\rangle|^2 \right)^{-1} \rightarrow \infty , \qquad (39)$$

is equivalent to Eq. (35). Note that this is true only if the scatterers are pointlike. By applying the eigenspace analysis of MUSIC (multiple signal classification) [65] to the discrete time reversal operator, Lev-Ary and Devaney [66] have developed a method, here referred to as time reversal and MUSIC (TRM), which also leads to condition (39). The equivalence between the methods has been clarified recently [67,68]. However, while the super resolving capabilities of the LSM and FM have not been pointed out so far, those of TRM have been discussed in a number of theoretical papers [69–71] along with the effects of multiple scattering [72]. Moreover, Prada and Thomas [73] have reported on a super resolution ultrasonic experiment performed in water with a linear array of sensors. The authors were able to separate two thin wires placed at 100λ from the array with a separation distance of $\lambda/3$, although no super resolved images of the two wires were provided in the paper.

VII. EXPERIMENTS

Since the possibility of achieving super resolution relies on the solution to an ill-posed problem it is crucial to investigate the role of noise and the extent to which it can compromise the resolution. Although the effect of noise can be simulated numerically, it was decided to perform an experimental investigation so as to assess how realistic the theoretical model used throughout the paper is. For this purpose a laboratory experiment was set up using elastic waves propagating in a metallic plate. It should be stressed that the setup was intended for a demonstration of super resolution under the presence of relatively high noise levels (current array technology can dramatically reduce the level of noise observed in this paper).

A. Setup

The experiments were performed on a square mild steel plate 1.25×1.25 m, 0.9 mm thickness, which represents the background medium shown in Fig. 1. The object to be imaged was simulated by means of two 3-mm-diameter, 26-mm-length steel rods bonded on one side of the plate, the distance between the rod centers being 4.7 mm as shown in Fig. 3. In order to measure the T_∞ operator a 57-element linear array, 280-mm aperture, 5-mm transducer interspace, was mimicked by positioning a single excitation transducer at 57 positions along the array "virtual" aperture. At each excitation location, the signal was detected at 57 positions corresponding to each array element. Therefore all the possible transmit and receive permutations of the array were collected (57×57 time traces). The distance between the virtual aperture and the rods was 115 mm. The probing wave was the fundamental flexural mode [74] A_0, whose phase velocity dispersion curve is shown in Fig. 4. The dispersion was measured experimentally so as to have an accurate estimate of the wavelength at different frequencies; the measurements being in excellent agreement with the Kirchhoff theory for thin plates [74] (the solid line curve is calculated with typical material properties of mild steel [75]: elastic modulus 210 GPa, Poisson's ratio 0.29, density 7800 kg/m^3). As can be deduced from Fig. 4, at 42 kHz, the wavelength is 14.3 mm which is slightly larger than three times the distance between the two rods. This frequency will be considered to estimate the resolution of the FM and TRM. Note that at this frequency the rod diameter is roughly $\lambda/5$; therefore the rods cannot strictly be regarded as pointlike scatterers. A_0 was excited by means of a piezoelectric disk, 5-mm diameter, 2-mm thickness with a brass backing mass of the same diameter, of 6 mm length. The mode was de-

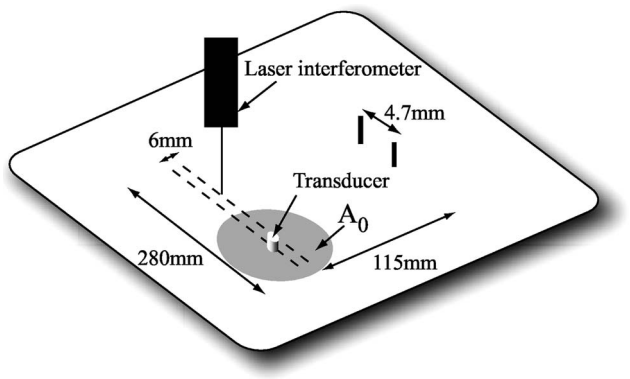

FIG. 3. Diagram of the experimental setup.

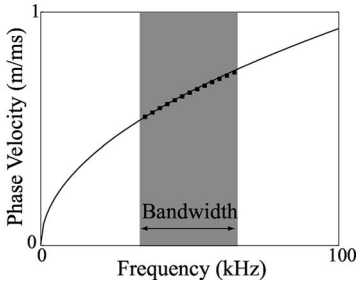

FIG. 4. Phase velocity dispersion curve of A_0. (square dots) Experiments; (solid line) Kirchhoff thin plate theory. The shading indicates the bandwidth of the wave packet.

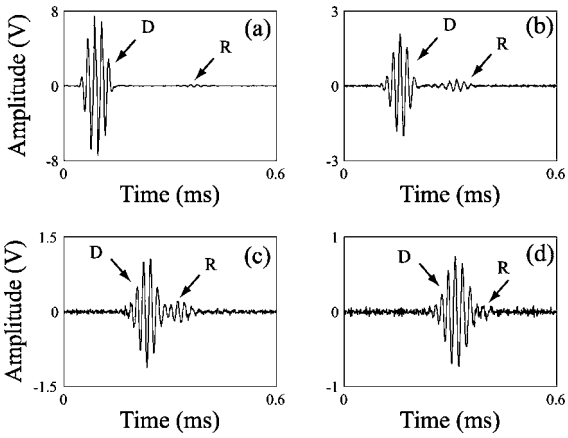

FIG. 5. Time domain signals recorded by the virtual array by firing one of the outer transducers and receiving: (a) in front of the transmitter; (b) 90 mm from the transmitter; (c) 185 mm from the transmitter; (d) 280 mm from the transmitter. D indicates the direct transmission from the exciter to the receiver and R the wave scattered from the targets.

tected with a laser interferometer (Polytec OFV 505) by orienting the laser beam perpendicularly to the plate so as to measure the out of plane component of the displacement. The transducer was excited by means of a custom-made wave-form generator-power amplifier with a five cycle Hanning windowed toneburst at 50 kHz center frequency, with a bandwidth of 30 kHz as shown in Fig. 4. The signal detected by the interferometer was averaged (200 times), amplified and sent to an oscilloscope for digital capture and subsequently stored in a PC.

The setup reproduces a two-dimensional limited view reconstruction problem. The problem can be considered to be two-dimensional because the wavelength is much larger than the plate thickness, as also confirmed by the agreement between the measured phase velocity and prediction from Kirchhoff theory. Moreover, since the aperture of the virtual array is limited the T_∞ operator can be sampled on a limited subset of $\mathbb{S}$ only. The main advantage of using a two-dimensional background is the possibility of mapping the wave fields directly by scanning the laser beam along the plate surface.

B. Scattered field

Figure 5 shows four of the 57×57 recorded signals, which were measured by exciting one of the outer transducers of the virtual array and receiving the signals at four equally spaced positions along the array aperture. In particular, Fig. 5(a) is the signal recorded in front of the transmitter. The larger signal (labeled D) is the outgoing wave traveling directly from the transmitter to the receiver while the lower signal arriving roughly 0.2 ms later, is the reflection from the two scatterers (labeled R). The transmitter behaves as a point source which excites a cylindrical wave corresponding to the two-dimensional Green's function [76]

$$G(\mathbf{r},\mathbf{r}') = -\frac{i}{4}H_0^{(1)}(k|\mathbf{r}-\mathbf{r}'|), \tag{40}$$

where $H_0^{(1)}$ is the Hankel function of order zero and type 1 [30], and $k=\omega/C_{ph}$ where C_{ph} is the phase velocity given in Fig. 4. As the monitoring point moves away from the transmitter, the amplitude of the outgoing signal D decreases rapidly [see Figs. 5(a)–5(d); note that the vertical scales are different for each plot]. Moreover, as the distance between the transmitter and receiver increases D tends to overlap the reflected signal R [Fig. 5(d)] making the separation of the two signals increasingly difficult.

The scattering of A_0 from the two rods can be studied with the same techniques used in acoustic or electromagnetic problems. In particular, since the wavelength is much larger than the plate thickness, each rod can be treated as a cylindrical inclusion with the same diameter as that of the rod and as thick as the plate; the inclusion being much stiffer than the plate so as to account for the additional inertia induced by the rod mass [77]. The main complication with flexural waves is that their propagation is described by a fourth order differential equation [74] which requires four boundary conditions to be satisfied at the inclusion-plate interface, by contrast with the two conditions required by the Helmholtz equation. This introduces some differences in the far-field pattern of a scattered flexural wave compared to that of an acoustic wave, although important properties such as the optical theorem remain unchanged [77].

In order to estimate the resolution a monochromatic analysis was performed. For each of the 3249 time traces, the scattered signal was isolated by gating out the direct transmission with a temporal end of gate calculated according to the relative distance between the transmitter and receiver and the group velocity of the A_0 wave packet. While this procedure is effective when the two signals are well resolved in time [Figs. 5(a) and 5(b)] it leads to severe errors when the signals overlap [Figs. 5(c) and 5(d)]. The reflected signal so obtained was subsequently Fourier transformed and for each frequency the data was stored in a 57×57 matrix, which is the multistatic matrix described by Devaney [69] and which corresponds to the discretization of the T_∞ operator.

C. Super resolved images

The eigenspace analysis described in Sec. VI was applied to the discretized T_∞ operator using the Tikhonov regularization based on the Morozov generalized discrepancy principle [57]. Figure 6(a) shows the FM pseudospectrum calculated at 42 kHz over an area of $3\lambda\times3\lambda$ around the scatterers, the circles indicating the scatterer actual positions and diameters. Although the scatterers were in the far-field of the probing system (8λ from the array virtual aperture), the FM can clearly achieve a resolution better than $\lambda/3$, as also shown in Fig. 6(b) which is a cross section of the pseudospectrum along the direction joining the scatterer centers. Note that for the experimental configuration of Fig. 3 the resolution limit dictated by the Rayleigh criterion [4] would be 11.3 mm.

This is a remarkable result for two reasons. First, the FM leads to a super resolved image despite the fact that the con-

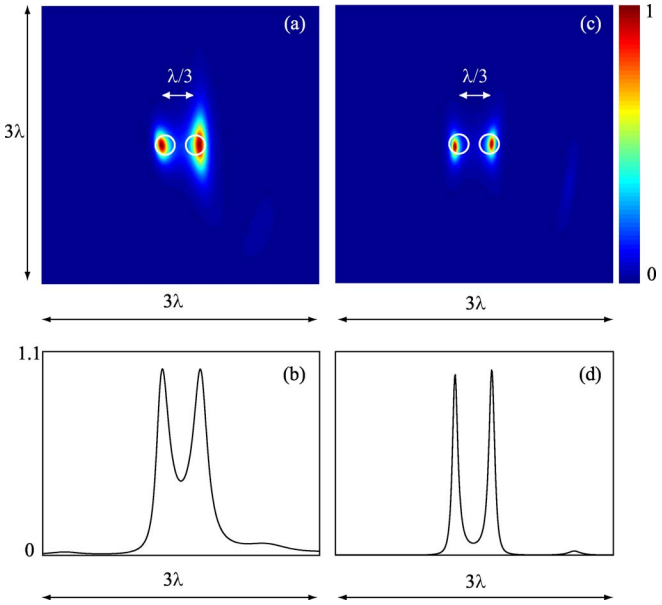

FIG. 6. (Color online) Super resolved images at 42 kHz over a $3\lambda \times 3\lambda$ area around the two scatterers, their cross sections being represented by the circles: (a) factorization method (FM); (b) cross section of the FM pseudospectrum along the direction joining the two scatterer centers; (c) time reversal and MUSIC method (TRM); (d) cross section of the TRM pseudospectrum.

dition of unitarity of the T_∞ operator, on which the FM heavily depends [57], is violated as the scattered field is measured over a limited aperture. Second, the experimental data exhibit a high level of noise. It is difficult to give an absolute estimate of the signal to noise ratio (SNR) since the noiseless T_∞ operator is unknown. One possibility is to base a noise estimate on the degree of asymmetry of the measured T_∞, which is assumed to be symmetric in the FM by a reciprocity argument. Therefore an averaged measure of the SNR (ASNR) can be expressed as

$$(\mathrm{ASNR}) = \frac{1}{N(N-1)} \sum_{i=1}^{N-1} \sum_{j=i+1}^{j=N} \frac{t_{ij} + t_{ji}}{t_{ij} - t_{ji}}, \tag{41}$$

where t_{ij} represents the amplitude of the signal recorded by the receiver at the ith location when the transmitter is at the jth position. The ASNR for the measured T_∞ was found to be 9.73 dB with a standard deviation of 13.0 dB. Similarly, the averaged phase noise was 0.2 rad with a standard deviation of 1.8 rad. There are two main reasons for such a high level of noise. First, since the laser detector cannot measure A_0 through the transmitter, the scanning direction of the laser was offset by 6 mm with respect to the scanning direction of the transmitter (see Fig. 3). As a result, the transmitter and receiver positions for the t_{ij} measurement were different from those of the t_{ji} measurement, hence the nonsymmetry of the data. The second source of error was the gating procedure previously described which leads to severe errors when the distance between the transmitter and receiver is large relative to the distance of the targets from the array. Although these sources of noise can be removed by using a real array of transmit-receive elements and a base-line subtraction approach to avoid the gating procedure, the result shown in Figs. 6(a) and 6(b) proves that the FM is robust against noise.

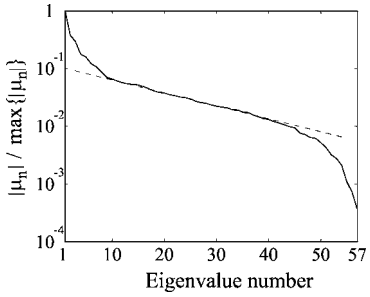

FIG. 7. Normalized eigenvalues of the T_∞ operator.

The image shown in Fig. 6(a) is the first experimental evidence of super resolution imaging with elastic waves. Prada and Thomas [73] have reported on a similar experiment which enabled the subwavelength detection of two thin wires immersed in water using acoustic waves (note that in this paper the probing fields are elastic waves). However, their results were obtained with the TRM method, which is based on the *a priori* knowledge of the pointlike nature of the scatterers, which therefore leads to a super resolved localization of known targets rather than super resolution imaging of an unknown scatterer shape. On the other hand, the FM does not require any *a priori* knowledge about the shape or number of the scatterers and Fig. 6(a) truly is an image of the scatterers.

For comparison, Figs. 6(c) and 6(d) provide the pseudospectrum of TRM obtained by applying Eq. (39) to the same T_∞ operator used to construct the FM image. The TRM image is extremely sharp and the location of the scatterer centers is very well defined. As observed in Sec. VI, the TRM pseudospectrum should be constructed by using the eigenvectors with zero eigenvalue only [Eq. (39)]. In practice, due to the presence of noise and the finite size of the scatterers none of the eigenvalues vanishes. Indeed, since the scatterers are equivalent to stiff cylindrical inclusions with a diameter of roughly $\lambda/5$, an infinite number of nonzero eigenvalues can be associated with each scatterer. However, as shown by Chambers and Gautesen [78] a finite number of them (four for a spherical inclusion) have dominant magnitude compared to the others. Therefore the TRM spectrum can be constructed by using the eigenvectors corresponding to the nondominant eigenvalues. Figure 7 provides the 57 eigenvalues of the measured T_∞ operator on a semilogarithmic scale, their values being normalized with respect to the largest eigenvalue. The criterion adopted in this paper to separate the dominant eigenvalues from the nondominant ones is based on the variations of the slope, or second order derivative, of the curve shown in Fig. 7. The point where the slope of the curve becomes constant is assumed to mark the transition between dominant and nondominant eigenvalues. Above the tenth eigenvalue the slope is almost constant as shown by the dashed line in Fig.7 therefore it is concluded in this case there are ten dominant eigenvalues. The steep variation of the slope observed above the 45th eigenvalue is due to the combination of noise and the relatively small ampli-

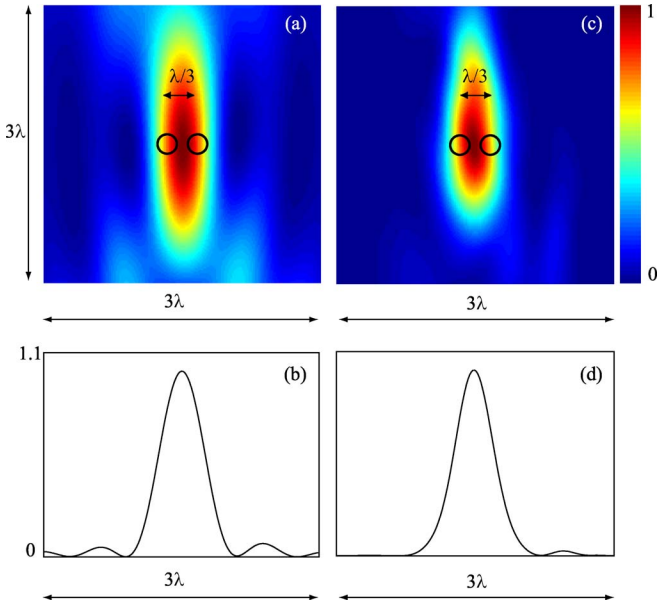

FIG. 8. (Color online) Images obtained with conventional techniques at 42 kHz: (a) DORT image; (b) DORT cross section; (c) synthetic phased array (SPA) image; (d) SPA cross section.

tude of the eigenvalues, so it is not considered. The image shown in Figs. 6(c) and 6(d) was obtained using the eigenvectors corresponding to the last 47 eigenvalues in Fig. 7. Note that TRM does not require any *a priori* knowledge about the number of scatterers, though the choice of the criterion to separate the eigenvalues is somehow arbitrary (see Ref. [79] and references therein).

Although in Sec. VI it was observed that for pointlike scatterers the FM and TRM are equivalent, the images shown in Figs. 6(a) and 6(c) differ from each other due to the finite size of the scatterers. TRM achieves a very high resolution in the location of the scatterer centers since it assumes they are pointlike, which enables to select the eigenvectors to be used to build the TRM spectrum by discarding those corresponding to dominant eigenvalues. However, TRM is limited to the imaging of pointlike scatterers and cannot image finite objects. On the other hand, the FM which can reconstruct finite objects (as also shown experimentally [57,68]) does not require any *a priori* knowledge about the number or shape of the scatterers (all the eigenvectors of the T_∞ operator are used) and provides a more general imaging method.

D. Conventional imaging

In order to further assess the super resolving capabilities of the FM and TRM a comparison with diffraction limited techniques was performed. Figure 8(a) shows a monochromatic image at 42 kHz obtained with the DORT algorithm [73]. The same set of data as in the previous reconstructions was used. The image is constructed by backpropagating the eigenvector with the largest eigenvalue [73]. Although DORT is able to detect the presence of the two targets it cannot resolve them [see also cross section in Fig. 8(b)], this being expected since the distance between the targets is subwavelength.

A second comparison was carried out with phased array imaging, which is one of the techniques commonly employed for limited view sensing. In typical medical or radar applications, a wave beam is focused and steered by applying a suitable phasing between the array elements. The volume to be imaged is sampled over a grid of points at which the beam is focused. At each point the image is proportional to the intensity of the reflected wave field at that point. The focusing can be done electronically by applying suitable time delays to each array element, or synthetically from the T_∞ operator [80]. While for nondispersive waves synthetic focusing is done in the time domain, the large dispersion of A_0 requires a different phasing law for each frequency carried by the wave packet. One possibility is to construct a series of monochromatic images for each frequency of the signal bandwidth, the final image being given by the superimposition of all the monochromatic components [81]. Figures 8(c) and 8(d) show the monochromatic image and its cross section at 42 kHz obtained with the angular spectrum method [81]. As for the DORT image, synthetic focusing enables the detection of the presence of the targets but it is not possible to separate them. A negligible improvement was observed by combining different frequencies. This is not surprising considering that, at each frequency, synthetic focusing provides an almost complete coverage of the Ewald sphere so making the information carried by different frequencies redundant as shown by Chiao and Thomas [82].

VIII. CONCLUSIONS

This paper has investigated the possibility of retrieving the subwavelength structure of an object by using diffracting waves excited and detected in the far-field. Classical reconstruction techniques model the interaction between the probing wave and the object by neglecting the distortion of the wave field induced by the object structure as the wave travels through it. The validity of this approximation is based on the assumption that the object is weakly scattering, however, this condition can be difficult to obtain in practice since it depends not only on the object contrast but also on the object size relative to the wavelength. In this paper it is emphasized that this approximation results in the classical resolution limit and it is shown that the distortion of the wave field, which is caused by multiple scattering within the object, encodes subwavelength information in the far-field pattern of the scattered wave. In other words, a single far-field measurement depends on all the spatial frequencies of the object rather than a limited subset of them. By reinterpreting the T-matrix formalism in the light of the reconstruction problem a direct relationship between far-field measurements and the subwavelength structure of the probed medium has been derived.

The theoretical argument has been applied to the shape reconstruction problem since the intrinsically nonlinear imaging problem can now be substituted by a linear integral equation which leads to a direct solution to the inverse prob-

lem. It has been observed that the linear sampling method and the factorization method can lead to super resolution imaging. The feasibility of super resolution has been supported by a limited view experiment performed with elastic waves in a metallic plate, for which a resolution better than $\lambda/3$, obtained without using *a priori* knowledge about the scatterer shape, is reported.

ACKNOWLEDGMENTS

The author is grateful to Professor P. Cawley and Dr. M. J. S. Lowe for critical reading of the manuscript and for many stimulating discussions. This work was supported by the UK Royal Academy of Engineering/Engineering and Physical Sciences Research Council.

[1] P. N. T. Wells, Rep. Prog. Phys. **62**, 671 (1999).
[2] A. J. Devaney, IEEE Trans. Geosci. Remote Sens. **GE-22**, 3 (1984).
[3] A. J. Devaney, Inverse Probl. **5**, 501 (1989).
[4] J. W. Goodman, *Introduction to Fourier Optics* (McGraw-Hill, New York, 1996).
[5] J. B. Pendry, Phys. Rev. Lett. **85**, 3966 (2000).
[6] E. Wolf, Opt. Commun. **1**, 153 (1969).
[7] E. Wolf and J. T. Foley, Opt. Lett. **23**, 16 (1998).
[8] E. H. Synge, Philos. Mag. **6**, 356 (1928).
[9] E. A. Ash and G. Nicholls, Nature (London) **237**, 510 (1972).
[10] A. Lewis, M. Isaacson, A. Harootunian, and A. Muray, Biophys. J. **41**, 405 (1983).
[11] U. Dürig, D. W. Pohl, and H. Rohrer, J. Appl. Phys. **59**, 3318 (1986).
[12] E. Betzig, J. K. Trautman, T. D. Harris, J. S. Weiner, and R. L. Kostelak, Science **251**, 1468 (1991).
[13] A. Lewis, H. Taha, Strinkovski, A. Manevitch, A. Khatchatouriants, R. Dekhter, and E. Ammann, Nat. Biotechnol. **21**, 1378 (2003).
[14] D. Courjon, *Near-field Microscopy and Near-field Optics* (Imperial College Press, London, 2003).
[15] J.-J. Greffet and R. Carminati, Prog. Surf. Sci. **56**, 133 (1997).
[16] D. Courjon and C. Bainier, Rep. Prog. Phys. **57**, 989 (1994).
[17] F. C. Chen and W. C. Chew, Appl. Phys. Lett. **72**, 3080 (1998).
[18] T. J. Cui, W. C. Chew, X. X. Yin, and W. Hong, IEEE Trans. Antennas Propag. **52**, 1398 (2004).
[19] K. Belkebir, P. C. Chaumet, and A. Sentenac, J. Opt. Soc. Am. A **22**, 1889 (2005).
[20] S. P. Carney and J. C. Schotland, J. Opt. Soc. Am. A **20**, 542 (2003).
[21] M. Fink, Phys. Today **50**(3), 34 (1997).
[22] P. Blomgren, G. Papanicolaou, and H. Zhao, J. Acoust. Soc. Am. **111**, 230 (2002).
[23] P. C. Waterman, J. Acoust. Soc. Am. **45**, 1417 (1968).
[24] D. Colton, Inverse Probl. **47**, 67 (2003).
[25] M. Born and E. Wolf, *Principles of Optics* (Cambridge University Press, Cambridge, England, 1999).
[26] O. Pade and A. Mandelis, Inverse Probl. **10**, 185 (1994).
[27] A. C. Kak, M. Slaney, *Computerized Tomographic Reconstruction* (IEEE Press, New York, 1999).
[28] L. S. Rodberg and R. M. Thaler, *The Quantum Theory of Scattering* (Academic Press, New York, 1967).
[29] R. W. James, *The Optical Principles of the Diffraction of X-rays* (G. Bell & Sons, London, 1948).
[30] G. B. Aarfken and H. J. Weber, *Mathematical Methods for Physicists* (Academic Press, London, 2001).
[31] M. Bertero and P. Boccacci, Micron **34**, 265 (2003).
[32] T. Habashy and E. Wolf, J. Mod. Opt. **41**, 1679 (1994).
[33] C. K. Rushforth and R. W. Harris, J. Opt. Soc. Am. **58**, 539 (1968).
[34] D. Slepian and H. O. Pollak, Bell Syst. Tech. J. **40**, 43 (1961).
[35] G. Toraldo Di Francia, J. Opt. Soc. Am. **59**, 799 (1969).
[36] S. P. Carney and J. C. Schotland, Appl. Phys. Lett. **77**, 2798 (2000).
[37] J.-J. Greffet, A. Sentenac, and R. Carminati, Opt. Commun. **116**, 20 (1995).
[38] G. S. Agarwal, Pure Appl. Opt. **7**, 1143 (1998).
[39] D. G. Fischer, J. Mod. Opt. **47**, 1359 (2000).
[40] A. Schatzberg and A. J. Devaney, Inverse Probl. **8**, 149 (1992).
[41] S. P. Carney and J. C. Schotland, Inverse Probl. **47**, 133 (2003).
[42] S. P. Carney and J. C. Schotland, Opt. Lett. **26**, 1072 (2003).
[43] J. Hadamard, *Lectures on Cauchy's Problem in Linear Partial Differential Equations* (Yale University Press, New Haven, CT, 1923).
[44] A. J. Devaney, Opt. Lett. **6**, 374 (1981).
[45] M. Azimi and A. C. Kak, IEEE Trans. Med. Imaging **MI-2**, 176 (1983).
[46] M. L. Oristaglio, J. Opt. Soc. Am. A **2**, 1987 (1985).
[47] B. Chen and J. J. Stamnes, Appl. Opt. **37**, 2996 (1998).
[48] M. I. Sancher and A. D. Varvatsis, Proc. IEEE **58**, 140 (1970).
[49] M. Slaney, A. C. Kak, and L. E. Larsen, IEEE Trans. Microwave Theory Tech. **MIT-32**, 860 (1984).
[50] F. Natterer, Inverse Probl. **20**, 447 (2004).
[51] E. Wolf and M. Nieto-Vesperinas, J. Opt. Soc. Am. A **2**, 886 (1985).
[52] A. Tikhonov, Sov. Math. Dokl. **4**, 1035 (1963).
[53] D. Colton and R. Kress, *Inverse Acoustic and Electromagnetic Scattering Theory* (Springer-Verlag, Berlin, 1992), Vol. 93.
[54] R. D. Luke and R. Potthast, SIAM J. Appl. Math. **63**, 1292 (2003).
[55] R. Potthast, *Point Sources and Multipoles in Inverse Scattering Theory* (Chapman & Hall/CRC, London, 2001).
[56] W. C. Chew and Y. M. Wang, IEEE Trans. Med. Imaging **9**, 218 (1990).
[57] D. Colton, J. Coyle, and P. Monk, SIAM Rev. **42**, 369 (2000).
[58] D. Colton and A. Kirsch, Inverse Probl. **12**, 383 (1996).
[59] M. I. Kolobov and C. Fabre, Phys. Rev. Lett. **85**, 3789 (2000).
[60] A. Kirsch, Inverse Probl. **14**, 1489 (1998).
[61] C. Prada, J. L. Thomas, and M. Fink, J. Acoust. Soc. Am. **99**, 2067 (1996).
[62] T. D. Mast, A. I. Nachman, R. C. Waag, J. Acoust. Soc. Am. **102**, 715 (1997).

[63] S. Li and E. J. Heller, Phys. Rev. A **67**, 032712 (2003).
[64] M. Lax, Rev. Mod. Phys. **23**, 287 (1951).
[65] R. O. Schmidt, IEEE Trans. Antennas Propag. **AP-34**, 276 (1986).
[66] H. Lev-Avri and A. J. Devaney, in *Sensor Array and Multichannel Signal Processing Workshop*, 2000, pp. 509–513.
[67] M. Cheney, Inverse Probl. **17**, 591 (2001).
[68] A. Kirsch, Inverse Probl. **18**, 1025 (2002).
[69] A. J. Devaney, IEEE Trans. Antennas Propag. **53**, 1600 (2005).
[70] S. K. Lehman and A. J. Devaney, J. Acoust. Soc. Am. **113**, 2742 (2003).
[71] T. Miwa and I. Arai, IEEE Trans. Antennas Propag. **52**, 220 (2004).
[72] F. K. Gruber, E. A. Marengo, and A. J. Devaney, J. Acoust. Soc. Am. **115**, 3042 (2004).
[73] C. Prada and J. L. Thomas, J. Acoust. Soc. Am. **114**, 235 (2003).
[74] K. F. Graff, *Wave Motion in Elastic Solids* (Clarendon Press, Oxford, 1975).
[75] G. W. C. Kaye and T. H. Laby, *Tables of Physical and Chemical Constants* (Longman, Essex, England, 1995).
[76] R. L. Weaver and Y. Pao, J. Appl. Mech. **49**, 821 (1982).
[77] A. N. Norris and C. Vemula, J. Sound Vib. **181**, 115 (1995).
[78] D. H. Chambers and A. K. Gautesen, J. Acoust. Soc. Am. **109**, 2616 (2001).
[79] H. Krim and M. Viberg, IEEE Signal Process. Mag. **13**, 67 (1996).
[80] M. Karaman, P.-C. Li, and M. O'Donnell, IEEE Trans. Ultrason. Ferroelectr. Freq. Control **42**, 429 (1995).
[81] R. Sicard, A. Chahbaz, and J. Goyette, IEEE Trans. Ultrason. Ferroelectr. Freq. Control **51**, 1287 (2004).
[82] R. Y. Chiao and L. J. Thomas, IEEE Trans. Ultrason. Ferroelectr. Freq. Control **41**, 484 (1994).